

# Nanoscale

Accepted Manuscript



This is an *Accepted Manuscript*, which has been through the Royal Society of Chemistry peer review process and has been accepted for publication.

*Accepted Manuscripts* are published online shortly after acceptance, before technical editing, formatting and proof reading. Using this free service, authors can make their results available to the community, in citable form, before we publish the edited article. We will replace this *Accepted Manuscript* with the edited and formatted *Advance Article* as soon as it is available.

You can find more information about *Accepted Manuscripts* in the [Information for Authors](#).

Please note that technical editing may introduce minor changes to the text and/or graphics, which may alter content. The journal's standard [Terms & Conditions](#) and the [Ethical guidelines](#) still apply. In no event shall the Royal Society of Chemistry be held responsible for any errors or omissions in this *Accepted Manuscript* or any consequences arising from the use of any information it contains.



## Carbon nanotubes as efficient hole collector for high voltage methylammonium lead bromide perovskite solar cells

Received 00th January 20xx,  
Accepted 00th January 20xx

DOI: 10.1039/x0xx00000x

www.rsc.org/

Zhen Li<sup>a</sup>, Pablo P. Boix<sup>a</sup>, Guichuan Xing<sup>b</sup>, Kunwu Fu<sup>a,c</sup>, Sneha A. Kulkarni<sup>a</sup>, Sudip K. Batabyal<sup>a</sup>, Wenjing Xu<sup>d</sup>, Anyuan Cao<sup>d</sup>, Tze Chien Sum<sup>b</sup>, Nripan Mathews<sup>a,c,e</sup> and Lydia Helena Wong<sup>a,c,e\*</sup>

A high open circuit voltage ( $V_{oc}$ ) close to 1.4 V under AM 1.5, 100 mW/cm<sup>2</sup> conditions is achieved when Carbon nanotubes (CNT)s is used as hole conductor in methyl ammonium lead bromide (MAPbBr<sub>3</sub>) perovskite solar cells. Time-resolved photoluminescence and impedance spectroscopy investigations suggest that the observed high  $V_{oc}$  is a result of the better charge extraction and lower recombination of CNT hole conductor. Tandem solar cells with all perovskite absorbers are demonstrated with MAPbBr<sub>3</sub>/CNTs top cell and MAPbI<sub>3</sub> bottom cell, achieving  $V_{oc}$  of 2.24 V in series connection. The semitransparent and high voltage MAPbBr<sub>3</sub>/CNTs solar cells show great potentials for applications of solar cell windows, tandem solar cells and solar driven water splitting.

### Introduction

Organic-inorganic metal halide perovskite, especially methylammonium lead halide or mixed halide, have drawn great attention in the photovoltaic community. With its excellent optoelectronic properties such as high absorption coefficient (>10<sup>4</sup> cm<sup>-1</sup>),<sup>[1]</sup> high mobility (25 Vs<sup>-1</sup>cm<sup>-1</sup>),<sup>[2]</sup> long and balanced carrier diffusion length (exceeding 100 nm),<sup>[3],[4]</sup> and low exciton binding energy,<sup>[5]</sup> MAPbI<sub>3</sub> perovskite solar cells have achieved efficiencies above 20% within a shorter period than other solar energy materials.<sup>[6]</sup> Efficient perovskite solar cells has been demonstrated with both meso-porous sensitized structure<sup>[7],[8]</sup> and planar heterojunction structure<sup>[9]</sup>, and fabricated by different deposition techniques such as single step deposition,<sup>[10]</sup> sequential deposition,<sup>[11]</sup> vacuum evaporation,<sup>[12]</sup> and gas transformation.<sup>[13]</sup> In the chemical composition aspect, substitutions or doping of organic cation<sup>[14],[15]</sup> and metallic,<sup>[16]</sup> halide element<sup>[17],[18]</sup> in the perovskite structure have been studied, showing great promises with the ability to tune the bandgap and electronic properties of the materials. Among all the chemical doping and substitutions, bromine based perovskite solar cells have shown some unique

properties such as high voltage,<sup>[19-21]</sup> semi-transparency and better stability.<sup>[17]</sup>

MAPbBr<sub>3</sub> with a large bandgap of 2.3 eV is not an optimal absorber for single junction solar cell. With a limited absorption range in the solar spectrum, the achievable photocurrent is below 9.7 mA/cm<sup>2</sup> according to Shockley–Queisser limit.<sup>[19]</sup> To compensate the low photocurrent, a higher voltage is needed to maintain decent performance. High photovoltage is favorable for voltage sensitive applications such as solar driven electrochemical energy storage, water electrolysis and electrocatalyst. To attain high voltage from the solar cell devices, electron and hole selective contacts need to be carefully selected and optimized. The commonly used hole transporting materials (HTM) in MAPbI<sub>3</sub> solar cell spiro-OMeTAD, is not compatible to deliver high  $V_{oc}$  in MAPbBr<sub>3</sub> solar cells due to the mismatch in band alignment. Therefore a broad range of HTMs has been investigated to tune the  $V_{oc}$  of the MAPbBr<sub>3</sub> solar cells,<sup>[20]</sup> and the highest  $V_{oc}$  attained was 1.51 V.<sup>[21]</sup> It is generally believed that HTM with HOMO level closer to the valence band of MAPbBr<sub>3</sub> (5.9 eV) could deliver higher  $V_{oc}$  in the solar cell.<sup>[20],[22]</sup> However, other properties of HTM such as carrier mobility, conductivity and kinetics of interfacial charge transfer and recombination could affect the  $V_{oc}$  of MAPbBr<sub>3</sub> solar cells as well. Therefore, HTM optimization is critical to achieve high voltage and efficiency in MAPbBr<sub>3</sub> solar cells.

Carbon materials, due to their excellent stability, low cost and facile processability, have been used to replace the expensive HTM and noble metal electrode in perovskite solar cells and achieved reliable efficiency and impressive stability.<sup>[23]</sup> Different forms of carbon have been demonstrated in constructing efficient perovskite solar cells,<sup>[24],[25]</sup> with

<sup>a</sup> Energy Research Institute @ NTU (ERI@N), Nanyang Technological University, Techno Plaza, 50 Nanyang Drive, 637553, Singapore.

<sup>b</sup> Division of Physics and Applied Physics, School of Physical and Mathematical Sciences, Nanyang Technological University, 637371, Singapore

<sup>c</sup> School of Materials Science and Engineering, Nanyang Technological University (NTU), Block N4.1, Nanyang Avenue, 639798, Singapore.

<sup>d</sup> Department of Materials Science and Engineering, College of Engineering, Peking University, Beijing 100871, People's Republic of China.

<sup>e</sup> Singapore-Berkeley Research Initiative for Sustainable Energy, 1 Create Way, 138602, Singapore.

Electronic Supplementary Information (ESI) available: [details of any supplementary information available should be included here]. See DOI: 10.1039/x0xx00000x

carbon nanotubes (CNTs) being a promising candidate due to its extraordinary electrical and mechanical properties.<sup>[26-28]</sup> Until now, most of these studies have focused on the MAPbI<sub>3</sub> system, however little is known about the interaction between carbon electrode and perovskite absorbers with different chemical compositions. With its outstanding conductivity, CNT electrode only needs a thin and transparent layer to transport holes in the solar cell. Therefore the transparent CNT electrode is a good combination with the semitransparent MAPbBr<sub>3</sub> absorber to form a suitable system with optimum applications in tandem solar cells and transparent solar cell windows among others.

Here, we have applied free standing carbon nanotubes films as hole conductor in MAPbBr<sub>3</sub> solar cells and achieved efficiencies up to 5.82%. The MAPbBr<sub>3</sub>/CNT solar cells have shown exceptionally high  $V_{OC}$  (up to 1.45 V), higher than solar cells with spiro-OMeTAD as HTM. Transient photoluminescence and impedance spectroscopy characterizations were conducted to investigate the interactions between MAPbBr<sub>3</sub> and CNTs, and the influences on the  $V_{OC}$  of solar cells. Finally, the transparent MAPbBr<sub>3</sub>/CNT solar cells were tested with double side illumination and assembled with a MAPbI<sub>3</sub> solar cell to demonstrate the concept of perovskite tandem solar cells.

## Experimental

### Substrate preparation and TiO<sub>2</sub> deposition

FTO glasses (Tec 7) were sequentially cleaned with decon soap solution, DI water, acetone, and absolute ethanol. Compact TiO<sub>2</sub> blocking layer was formed by screen printing of BL-1 paste from Dyesol followed by a TiCl<sub>4</sub> post treatment (100 mM, 30 min). Meso-porous TiO<sub>2</sub> layer was screen printed on the compact layer with a modified 30NRD paste from Dyesol. Both the compact and meso-porous TiO<sub>2</sub> layers were sintered at 500 °C for 30 min.

### Synthesis of free-standing carbon nanotube film

Carbon nanotubes were synthesized using a floating catalyst chemical vapor deposition method.<sup>[26]</sup> 0.651 g of ferrocene and 0.012 g of S was dissolved in 10 mL of xylene as precursors. The precursor solution was injected into a horizontal quartz tube furnace and carried by mixed gas of Ar and H<sub>2</sub> (2500/600 sccm) to 1160 °C reaction zone. After nucleation and growth in the gas flow, CNTs was brought downstream to the end of furnace (<200 °C), where they were collected by Ni foils and form free-standing thin films.

### MAPbBr<sub>3</sub> deposition and solar cell fabrication

MAPbBr<sub>3</sub> was deposited by spin coating with solvent engineering technique.<sup>[7]</sup> 1.2 M equal molar of CH<sub>3</sub>NH<sub>3</sub>Br and

PbBr<sub>2</sub> were dissolved in a mixed solvent of  $\gamma$ -butyrolactone and dimethyl sulfoxide (v:v=7:3) at room temperature. The solution was spin coated on the TiO<sub>2</sub> substrates with two step process: 4000 rpm for 20 s; followed by 6000 rpm for 10 s, 50  $\mu$ L of toluene was added to the substrate during the second step. Perovskite were annealed at 100 °C for 10 min after spin coating.

For MAPbBr<sub>3</sub>/CNT solar cells, MAPbBr<sub>3</sub> substrates were covered by free standing CNT films manually. The deposition process is shown by photos in Figure S1. Several drops of hexane were added to increase the adhesion of CNTs to the MAPbBr<sub>3</sub> surface. A thin layer of PMMA (20 mg/mL) was deposited on CNTs using spin coating (4000 rpm, 30s). To reduce the series resistance, gold finger electrode was deposited by thermal evaporation. The design of finger electrode was shown in supporting information (figure S2).

For standard MAPbBr<sub>3</sub>/spiro-OMeTAD solar cells, spiro-OMeTAD (100 mg/mL, Merck) in chlorobenzene was spin coated on the MAPbBr<sub>3</sub> substrates at 4000 rpm for 30 s. Dopants such as tBP (40  $\mu$ L), LiTFSi (24.2  $\mu$ L, 2 M acetonitrile solution), FK102 (12 mg in 40  $\mu$ L of acetonitrile) were added to the spiro-OMeTAD solution.

### Solar cell measurement and characterization:

The solar cells measurements were carried out using a solar simulator (San-Ei Electric, XEC-301S under AM 1.5 G condition), the light intensity was calibrated to 1 sun using a silicon standard cell (Newport). *J-V* curves were measured using a source meter (Keithley 2612A) with a scan rate of 100 mV/s (reversed scan). Active areas were defined by masks, 0.3 cm<sup>2</sup> for CNT cells and 0.2 cm<sup>2</sup> for spiro-OMeTAD cells. IPCE spectra were measured using a homemade system with a 300-W xenon lamp (ILC Technology) and Gemini-180 double monochromator (Jobin Yvon). The signal was recorded using a DSP lock-in amplifier (SR830, Stanford Research Systems) with a chopping frequency of 2 Hz, approximately. All measurements were conducted under a constant white light bias of 5 mW/cm<sup>2</sup> generated by an array of white light emitting diodes.

### Transient photoluminescence

The TRPL was conducted with femtosecond laser pulses generated from a Coherent Libra<sup>TM</sup> regenerative amplifier (50 fs, 1 KHz, 800 nm) seeded by a Coherent Vitesse<sup>TM</sup> oscillator (50 fs, 80 MHz). 800 nm laser pulses were from the regenerative amplifier's output while 400 nm laser pulses were obtained with a BBO doubling crystal. 450-nm laser pulses were generated from the Coherent OPerA-Solo optical parametric amplifiers. The emission from the samples was collected at a backscattering angle of 150° by a pair of lenses and into an Optronis Optoscope<sup>TM</sup> streak camera system which has an ultimate temporal resolution of ~10 ps.

## Results and discussion

Free standing carbon nanotube (CNT) film with single and few walled nanotubes were used as hole transport electrode. The CNT film was synthesized directly from chemical vapor deposition and used as grown. This CNT film owns intrinsic properties of pristine CNTs without surface functionalization. SEM images of the CNT network on the perovskite surface were shown in the supporting materials (Figure S3).

Figure 1a shows the fabrication procedures of MAPbBr<sub>3</sub>/CNT solar cells. A compact layer of TiO<sub>2</sub>, followed by a mesoporous TiO<sub>2</sub> layer were screen printed on FTO glass substrates. The compact TiO<sub>2</sub> layer with thickness of 30-50 nm serves as electron selective contact and hole blocking layer to MAPbBr<sub>3</sub> perovskite. Mesoporous TiO<sub>2</sub> with thickness of 300

nm was used as electron transport scaffold in the solar cells. After the mesoporous TiO<sub>2</sub> layer, MAPbBr<sub>3</sub> was deposited by spin coating using a solvent engineering method,<sup>5</sup> which applies a poor solvent of perovskite to the substrates during spin coating. The poor solvent induces fast crystallization of perovskite and forms a compact perovskite capping layer on top of TiO<sub>2</sub> (Figure S3). The attained perovskite absorber layer has a smooth and flat top surface and a capping layer with thickness of about 200 nm (figure 1b). The smooth surface enables more intimate contact between perovskite and porous carbon nanotube electrode, which would be beneficial in charge collection as compared to the rough surface produced by conventional single step deposition. As shown in figure 1b, the MAPbBr<sub>3</sub> absorber is a yellowish semi-transparent film with a large band gap of 2.3 eV.

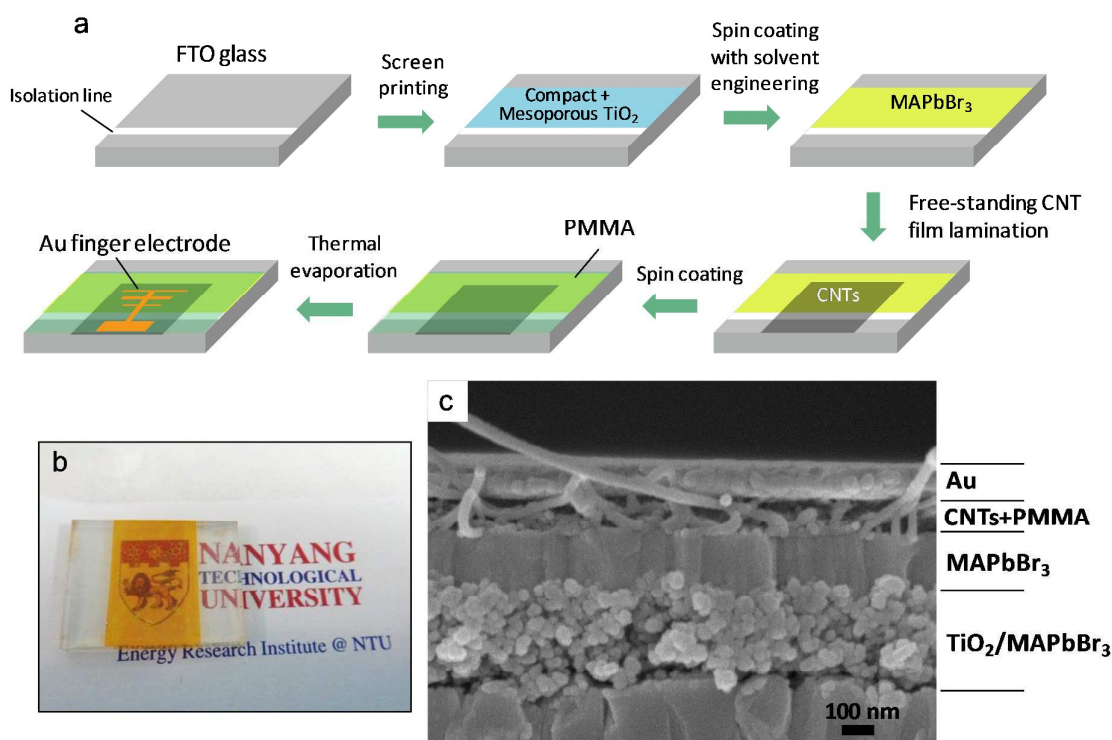


Figure 1. (a) Schematics of the fabrication procedures for MAPbBr<sub>3</sub>/CNT solar cells; (b) photo of semitransparent MAPbBr<sub>3</sub> absorber deposited on TiO<sub>2</sub> substrates; (c) Cross sectional SEM image of MAPbBr<sub>3</sub>/CNT solar cell with PMMA coating and Au electrode.

Though the solar cell performance can be measured after CNT coating, usually two more layers were deposited to improve the stability and performance of the solar cells. A thin layer of poly(methyl methacrylate) (PMMA) was spin coated on CNT film to improve the contact between CNTs and perovskite. The PMMA layer also acted as a barrier layer to

improve the stability of perovskite under layer.<sup>[27]</sup> A finger gold electrode was evaporated to reduce the series resistance of the CNT electrode and at the same time maintain some space for light to pass through. The design of the finger electrode is shown in figure S2.

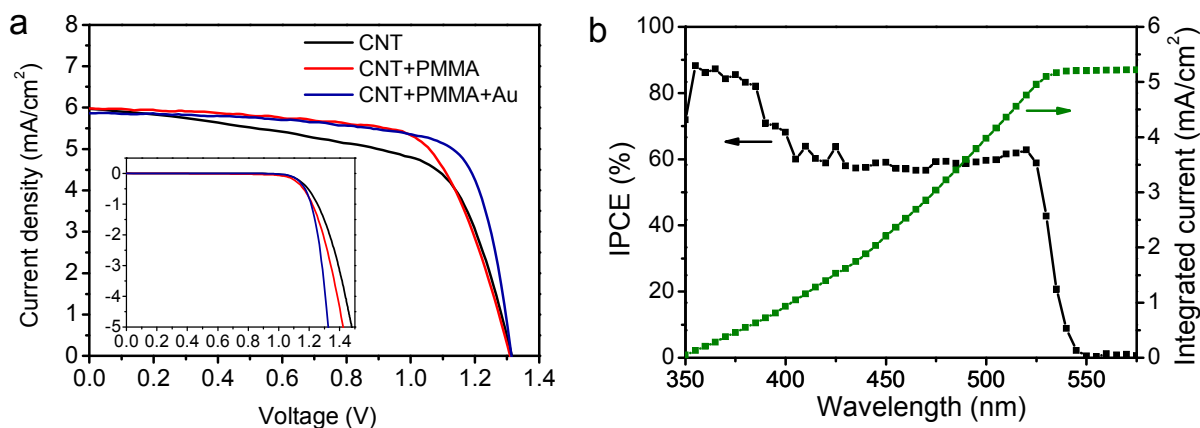


Figure 2. (a) Light J-V curve changes of a MAPbBr<sub>3</sub>/CNTs solar cell after PMMA coating and Au deposition (AM 1.5G, 1 sun); inset: dark J-V curves of the solar cells; (b) IPCE and integrated photocurrent of the MAPbBr<sub>3</sub>/CNTs solar cell.

Figure 2a shows a typical J-V characteristic of the solar cells under 1 sun illumination. The MAPbBr<sub>3</sub>/CNT solar cells showed little hysteresis in their J-V curves and very fast respond to light changes (Figure S4 and S5). Table 1 summarizes the performance parameters derived from the J-V curves. The solar cells performance improved after PMMA coating and Au evaporation, mainly due to the enhanced of fill factor. Meanwhile, the  $V_{OC}$  and  $J_{SC}$  remain nearly unchanged, even showing a slight decrease of  $J_{SC}$  after Au evaporation. The increase of fill factor can be explained by the change of series resistance ( $R_s$ ) in the solar cell.  $R_s$  is calculated from the slope of dark J-V curves (inset of figure 2b) and shown in table 1. After PMMA coating, shrinkage of PMMA polymer brought the stacking carbon nanotubes closer to the perovskite surface, reducing the contact resistance at the perovskite/CNT interface.

The  $R_s$  of solar cell further decreases from 34.3 to 13.0  $\Omega \text{ cm}^2$  after Au deposition. This suggests that one of the major obstacles using our CNT network as hole transporting electrode for perovskite solar cell is its high sheet resistance. The resistance can be reduced by increasing the CNT film thickness, which however will sacrifice the transparency of the electrode. The best performance solar cell was with PMMA coating and Au finger electrode, showing a  $V_{OC}$  of 1.31 V,  $J_{SC}$  of

5.86  $\text{mA/cm}^2$ , fill factor of 0.75 and power conversion efficiency of 5.82%. If not stated otherwise, solar cells with CNT hole conductor mentioned in the following discussions adapts this best performing structure with PMMA coating and Au finger electrode. PMMA coating acts as a barrier layer and protects the underlying MAPbBr<sub>3</sub> absorber layer. Therefore, there is not much degradation to the MAPbBr<sub>3</sub>/CNT solar cell stored in a dry desiccator for 45 days (Figure S6), showing decent device stability. Stability of the solar cells under more harsh conditions will be studied in the future.

Table 1. Photovoltaic parameters of MAPbBr<sub>3</sub>/CNTs solar cell with PMMA coating and Au finger electrode

	$V_{OC}$ (V)	$J_{SC}$ ( $\text{mA/cm}^2$ )	$FF$	$\eta$ (%)	$R_s$ ( $\Omega \text{ cm}^2$ )
CNTs	1.31	5.96	0.62	4.84	42.8
CNTs+PMMA	1.31	5.98	0.68	5.33	34.3
CNTs+PMMA+Au	1.31	5.86	0.75	5.76	13.0

Incident photon-to-electron conversion efficiency (IPCE) of the solar cell, together with the integrated photocurrent is shown in figure 2b. The IPCE of the MAPbBr<sub>3</sub>/CNT solar cell features a plateau between 400 to 525 nm with an IPCE of 60%. The attained IPCE edge is consistent with the absorption spectrum of MAPbBr<sub>3</sub>, which shows an optical band gap of 2.3 eV. Further improvement of IPCE is feasible by optimizing the deposition of MAPbBr<sub>3</sub> absorber.<sup>[28]</sup>

The commonly used hole transporting material spiro-OMeTAD, was employed to fabricate MAPbBr<sub>3</sub> solar cells for comparison. Figure 3a shows the typical light *J-V* curves of MAPbBr<sub>3</sub> solar cells with CNT and spiro-OMeTAD as hole

conductor. It is worth to mention that the  $V_{OC}$  of MAPbBr<sub>3</sub>/CNT solar cell exceeds the energetic difference between the TiO<sub>2</sub> conduction band and CNT work function (figure 3b). Similar result with voltage output exceeding the energetic difference of electron and hole selective contacts was also observed in previous reports.<sup>[22]</sup> This fact suggests that the perovskite itself plays an important role in building  $V_{OC}$  across solar cell device, probably by a splitting of the electron and hole Fermi levels within the absorber. Under these circumstances, processes such as charge separation and recombination within the perovskite layer gain importance in the determination of the achieved  $V_{OC}$  in the perovskite solar cells.

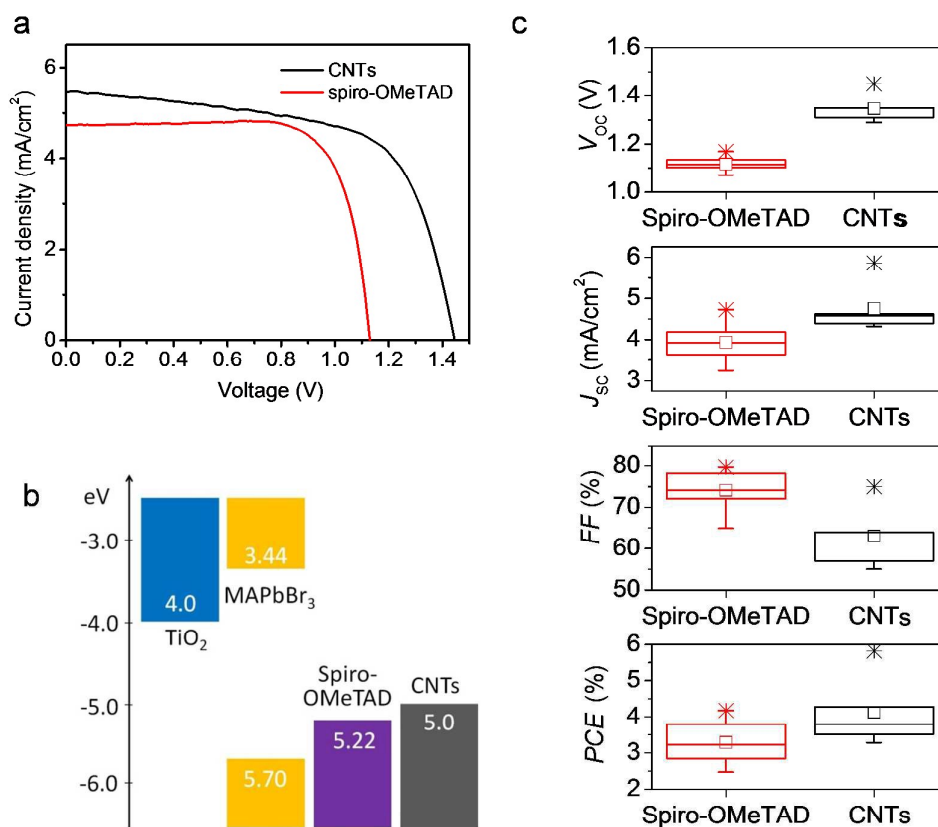


Figure 3. (a) Characteristic light *J-V* curves of MAPbBr<sub>3</sub> solar cells with CNTs and spiro-OMeTAD as hole conductors; (b) Energetic levels of materials in MAPbBr<sub>3</sub> solar cells; (c) Statistics evaluation of photovoltaic parameters of MAPbBr<sub>3</sub> solar cells from 20 spiro-OMeTAD cells and 10 CNT cells

The solar cell performance parameters are compared in figure 3c from statistical data of 20 spiro-OMeTAD cells and 10 CNT cells. The statistical data is shown in the form of box plots with the empty square symbol representing the average value, star symbol as the maximum value and middle bar of the box as the median of the data set. The average  $V_{OC}$  of CNT cells (1.35 V) is significantly higher than that of spiro-OMeTAD cells

(1.11 V). The highest  $V_{OC}$  attained by CNT cells is 1.45 V, which is among the highest  $V_{OC}$  attained by MAPbBr<sub>3</sub> solar cells.<sup>[20], [22]</sup> The average  $J_{SC}$  of CNTs cells is also slightly higher than that of spiro-OMeTAD counterparts (4.75 vs. 3.93 mA/cm<sup>2</sup>). The fill factors of CNT cells, in contrast, are lower with larger standard variation, presumably due to the larger sheet resistance and larger resistance variation from different batches of CNT films. Overall, the average power conversion efficiency of CNT cells is

higher than spiro-OMeTAD cells (4.12% vs. 3.28%), mainly due to higher  $V_{OC}$  of CNT cells.

In MAPbBr<sub>3</sub> based perovskite solar cells, HTM with deeper HOMO level usually produces higher  $V_{OC}$ . However, we systematically observed higher  $V_{OC}$  in MAPbBr<sub>3</sub>/CNT solar cells than in MAPbBr<sub>3</sub>/spiro-OMeTAD cells, even though the CNT work function (-5.0 eV) is higher than the HOMO level of spiro-OMeTAD (-5.22 eV). Recently, MAPbBr<sub>3</sub> perovskite solar cell without hole transporting materials was reported with a high

$V_{OC}$  of 1.35 V.<sup>[29]</sup> The high voltage was explained by lower surface potential of MAPbBr<sub>3</sub> than MAPbI<sub>3</sub>. Although consisted of both semiconductor and metallic nanotube, the mixture carbon nanotube network presented a semi-metal behavior with all the electronic state filled up to the Fermi level. Given the similarity of MAPbBr<sub>3</sub>/CNT and MAPbBr<sub>3</sub>/Au interface, it is reasonable to achieve high voltage in the MAPbBr<sub>3</sub>/CNT solar cells. To further interpret the attained high voltage in MAPbBr<sub>3</sub>/CNT solar cells, transient photoluminescence spectroscopy and impedance spectroscopy studies were conducted.

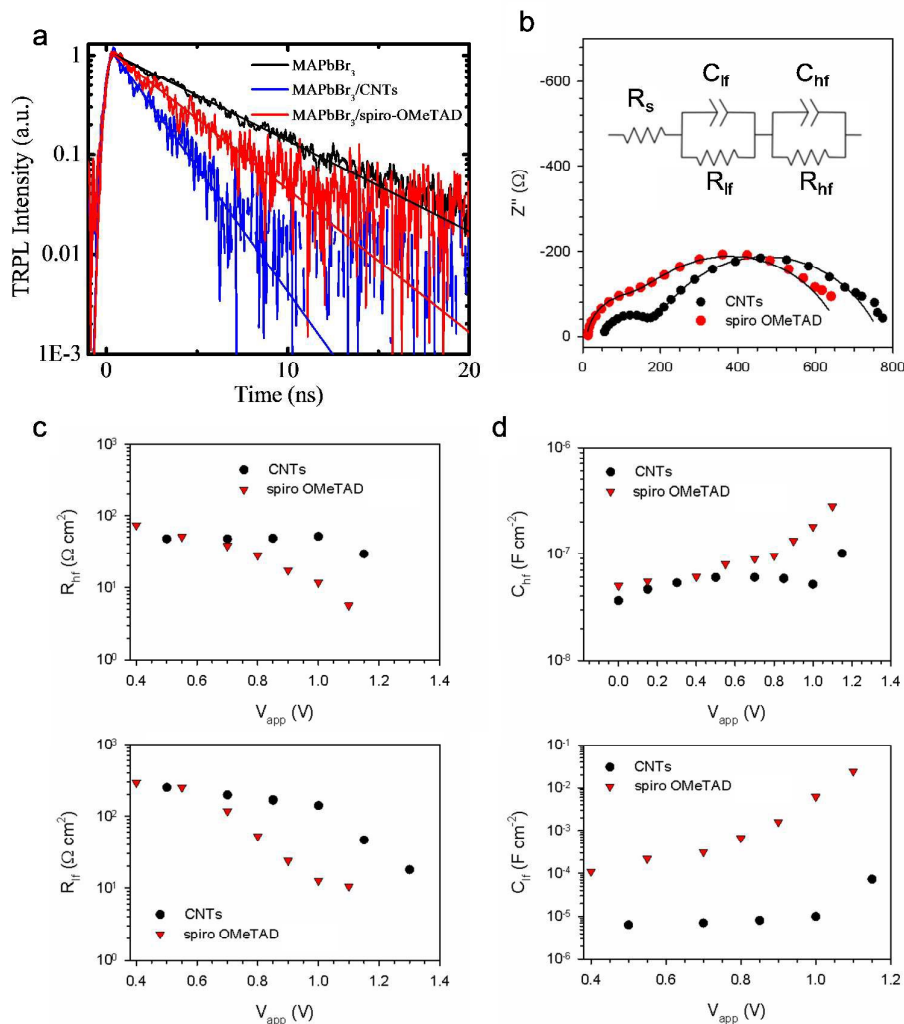


Figure 4. (a) Transient photoluminescence spectra of MAPbBr<sub>3</sub> coated with different hole transporting materials; (b) Impedance spectra for MAPbBr<sub>3</sub>/CNTs and MAPbBr<sub>3</sub>/spiro-OMeTAD solar cells under illumination and bias of 0.7 V, inset shows the equivalent circuit for parameter fitting; (c) Resistance extracted from impedance spectra for CNTs and spiro-OMeTAD cells; (d) Capacitance extracted from impedance spectra for CNTs and spiro-OMeTAD cells.

Figure 4a shows TRPL spectra of MAPbBr<sub>3</sub> films coated with CNT film and spiro-OMeTAD with a laser excitation wavelength of 450 nm. CNTs and spiro-OMeTAD both show strong PL quenching effect of MAPbBr<sub>3</sub>, due to hole extraction from the

excited MAPbBr<sub>3</sub> films. Figure 4 also shows that PL quenching of MAPbBr<sub>3</sub> is more pronounced with CNT than with spiro-OMeTAD. The PL lifetimes are  $4.8 \pm 0.1$  ns,  $1.7 \pm 0.1$  ns and  $3.0 \pm 0.1$  ns for MAPbBr<sub>3</sub>, MAPbBr<sub>3</sub>/CNT and MAPbBr<sub>3</sub>/spiro-OMeTAD, respectively. Stronger PL quenching effect of CNTs

indicates faster charge carrier extraction from MAPbBr<sub>3</sub> to CNT than to spiro-OMeTAD. The improved charge transfer process could reduce the charge recombination and thus imply a better  $V_{oc}$  in the solar cells.

Impedance spectra of CNT and spiro-OMeTAD cells were also measured under illumination. The former shows a spectrum with two main features separated in frequencies, the measurement of the latter cells resulted in more merged spectrum (Figure 4b). In both cases the results were fitted to a simplified equivalent circuit with two resistances in parallel to two capacitances (inset of figure 4b), where the high frequency resistance ( $R_{hf}$ ) is attributed to the hole transport and the low frequency resistance ( $R_{lf}$ ) represents the recombination.<sup>[30], [31]</sup> These parameters (figure 4c) show a higher  $R_{hf}$  for the CNT cells. Series resistance extracted from

the spectra (Figure S7) also showed higher  $R_s$  for CNT cells than spiro-OMeTAD cells with Au electrode. The high  $R_{hf}$  and  $R_s$  could be due to the high sheet resistance of CNT and justifies the lower FF of these cells. Interestingly,  $R_{lf}$  is significantly higher for the CNT cell, indicating a reduced recombination process enhancing the  $V_{oc}$ .

The behavior of the capacitances of the analyzed devices presents clear differences as well (Figure 4d). While the high frequency capacitances ( $C_{hf}$ ) of both devices are similar and almost invariant in all the voltage range, the low frequency capacitance ( $C_{lf}$ ) of the CNT device is much lower than the spiro-OMeTAD one. In addition, the rise of  $C_{lf}$  for the CNTs device is shifted to higher potentials. This is tentatively related to a different band alignment of the devices, which could be the reason of the higher  $V_{oc}$  and should be further studied.

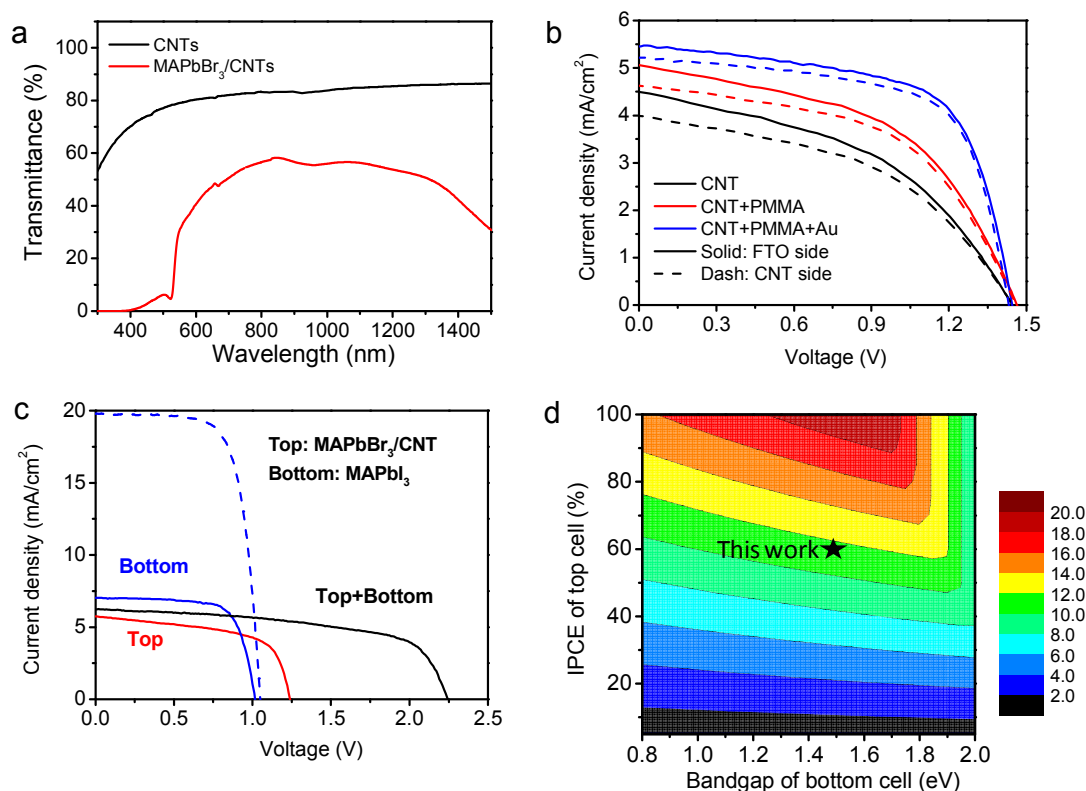


Figure 5. (a) UV-Vis transmittance spectra of CNT film and MAPbBr<sub>3</sub>/CNT solar cells; (b) Light J-V curves of MAPbBr<sub>3</sub>/CNT with different illumination direction\*; (c) Light J-V curves of tandem solar cell by stacking a transparent MAPbBr<sub>3</sub>/CNT (top) solar cell and a MAPbI<sub>3</sub> (bottom) solar cell and connected in series, dash curves represents MAPbI<sub>3</sub> solar cell before stacking; (d) Calculated tandem cell efficiency based on bandgap of bottom cell and IPCE of MAPbBr<sub>3</sub> top cell.

\*: Active area for CNT side illumination has excluded the area of Au grid electrode.

Table 2. Photovoltaic parameters of individual solar cells and tandem solar cells

	$V_{OC}$ (V)	$J_{SC}$ (mA/cm <sup>2</sup> )	$FF$	$\eta$ (%)
MAPbBr <sub>3</sub> /CNT (top)	1.24	5.75	0.61	4.33
MAPbI <sub>3</sub> (bottom)	1.02	7.02	0.72	5.13
Tandem (in series)	2.24	6.24	0.59	8.30
Tandem (4 wires)	—	—	—	9.46
MAPbI <sub>3</sub> original	1.05	19.8	0.71	14.8

The UV-Vis transmittance spectra of CNTs and MAPbBr<sub>3</sub>/CNT solar cells are shown in figure 5a. Transmittance of CNT is 60-80% in all the measured range. MAPbBr<sub>3</sub>/CNT solar cell showed a transmittance about 40-50% in the wavelength range from 600-1200 nm, and gradually dropping after 1200 nm. Figure S8 showed the photo of semi-transparent MAPbBr<sub>3</sub>/CNT solar cell with gold finger electrode.

Given the high transmittance of CNT electrode, MAPbBr<sub>3</sub>/CNT solar cells were tested with bi-facial illumination. The solid and dash curves of figure 5b represent the light J-V curves of the same solar cell with illumination coming from FTO and CNT side respectively. When illuminated from CNT side, the solar cell shows the same  $V_{OC}$ , but a slightly lower  $J_{SC}$  than illuminated from FTO side. Lower photocurrent may due to the lower transmittance of CNT. After the Au deposition, the  $J_{SC}$  attained from CNT side illumination is lower because light is partly blocked by the Au finger electrode. Table 2 summarizes the performance parameters of the solar cell with different side illumination.

The transparent MAPbBr<sub>3</sub>/CNT devices presents an opportunity to fabricate tandem solar cells. For demonstration, one MAPbI<sub>3</sub> solar cell (bottom cell) was physically stacked below a MAPbBr<sub>3</sub>/CNT solar cell (top cell). The top and bottom cells were separately tested and then tested in series connection. After stacking, the bottom MAPbI<sub>3</sub> cell produced  $V_{OC}$  of 1.02 V,  $J_{SC}$  of 7.02 mA/cm<sup>2</sup>,  $FF$  of 0.72 and  $PCE$  of 5.13%. The top MAPbBr<sub>3</sub> cell produced  $V_{OC}$  of 1.24 V,  $J_{SC}$  of 5.75 mA/cm<sup>2</sup>,  $FF$  of 0.61 and  $PCE$  of 4.33%. The MAPbI<sub>3</sub> cell could independently generate  $V_{OC}$  of 1.05 V,  $J_{SC}$  of 19.8 mA/cm<sup>2</sup>,  $FF$  of 0.71 and  $PCE$  of 14.8% before mounting below MAPbBr<sub>3</sub> cell (dash in figure 5c). The voltage of bottom and top cells were added up when the two cells were connected in series ( $V_{OC}$  of 2.24 V) and showed a  $J_{SC}$  of 6.24 mA/cm<sup>2</sup>,  $FF$  of 0.59 and  $PCE$  of 8.30%. The tandem cell  $J_{SC}$  is higher than the  $J_{SC}$  of MAPbBr<sub>3</sub> top cell because the J-V curve of the top cells has a non-plateau shape and the current is not saturated at the  $J_{SC}$  point. The combined cell efficiency was lower than the sum of two individual cells suggesting a large efficiency loss of the bottom cell in our non-optimized tandem cell configuration. This can be due to the current mismatch between top and bottom cells:  $J_{top}$  from MAPbBr<sub>3</sub> top cell was

lower than the  $J_{bottom}$  provided by MAPbI<sub>3</sub> bottom cell, thus limiting the achievable photocurrent out of the tandem cell.

In order to understand the limiting factor of our present configuration and direction for future optimization, tandem cell efficiency under ideal condition was simulated and plotted in figure 5d. The simulation was based on the following assumptions: transmittance of the top cell is 0% in the MAPbBr<sub>3</sub> absorption range and 80% above the MAPbBr<sub>3</sub> absorption range (transmittance of CNT film); IPCE of bottom cell is constantly 80% in all absorption range;  $V_{OC}$  of the MAPbBr<sub>3</sub> solar cell reaches an optimal value of 1.5 V and  $V_{OC}$  of the bottom cell has a constant  $V_{OC}$  deficit of 0.4 V,<sup>[32]</sup>  $FF$  reaches an optimal value of 0.7 for both the top and bottom cells. The resulting  $J_{SC}$ ,  $V_{OC}$ ,  $FF$  and  $PCE$  follow the equations as below:

$$J_{SC,series} = \min(J_{SC,top}, J_{SC,bottom})$$

$$V_{OC,series} = V_{OC,top} + V_{OC,bottom} \\ = 1.5 \text{ V} + \left( \frac{Eg_{bottom}}{eV} - 0.4 \text{ V} \right)$$

$$FF_{series} = FF_{top} = FF_{bottom} = 0.7$$

$$\eta_{series} = J_{SC,series} \times V_{OC,series} \times FF_{series}$$

As shown in figure 5d, the efficiency for series-connected cell increases with the IPCE of the top cell. The current of top cell is the limiting factor of the series solar cell. The MAPbBr<sub>3</sub> can generate a maximum  $J_{SC}$  of 9.8 mA/cm<sup>2</sup>, which is lower than half of the  $J_{SC}$  generated by a state of art MAPbI<sub>3</sub> solar cell (>20 mA/cm<sup>2</sup>), therefore  $J_{SC}$  provided by the bottom cell is excessive and wasted as mismatching current. The IPCE of the top cell was approximately 60% in our series tandem cell, as indicated with star symbol in figure 5d. The low IPCE could be due to high recombination rates in our MAPbBr<sub>3</sub> films as shown by the short PL lifetime. Improving film compactness and reducing grain boundaries in the MAPbBr<sub>3</sub> absorber layer could suppress the recombination and improve IPCE of the MAPbBr<sub>3</sub> solar cells. Boosting photocurrent of the top cell by

improving IPCE would lead to better tandem cell efficiency. Therefore, future optimization of the tandem cell configuration should focus on improving the photocurrent of the top cell or adjusting the top cell absorber with a smaller bandgap following previously reported mixed halide techniques.<sup>[17], [33]</sup>

## Conclusions

In conclusion, carbon nanotubes were used as hole conductor in MAPbBr<sub>3</sub> perovskite solar cells. With a facile process of directly transferring free-standing carbon nanotube networks onto MAPbBr<sub>3</sub> layer, solar cells can be fabricated without expensive hole transporting materials. The solar cell efficiencies were further improved by PMMA coating and Au grid electrode and reached up to 5.28%, under AM 1.5, 100 mW/cm<sup>2</sup> condition. The MAPbBr<sub>3</sub>/CNTs showed high open circuit voltage (Voc) with average of 1.35 V (maximum at 1.45 V), higher than solar cells using spiro-OMeTAD as HTM. Transient photoluminescence and impedance spectroscopy investigation suggested that better charge extraction efficiency and lower recombination of CNTs attributes to the observed high Voc. The semi-transparent, high voltage MAPbBr<sub>3</sub>/CNTs solar cells will show great potential in solar cell windows, tandem solar cells and solar fuels applications.

## Acknowledgements

The authors acknowledge the finance support from and financial support from the Singapore NRF through the Singapore-Berkeley Research Initiative for Sustainable Energy (SinBeRISE) CREATE program. G.C. Xing and T.C. Sum acknowledge the financial support from NTU start-up grant M4080514, SPMS collaborative Research Award M4080536, Ministry of Education AcRF Tier 2 grants MOE2013-T2-1-081 and MOE2014-T2-1-044. The authors also want thank Nancy Jiang for experiments and discussions.

## References

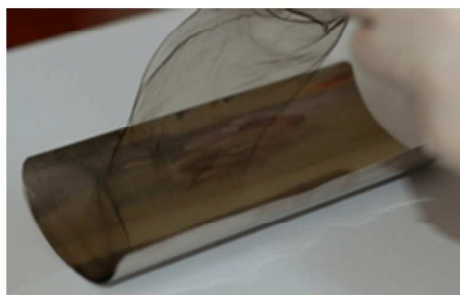
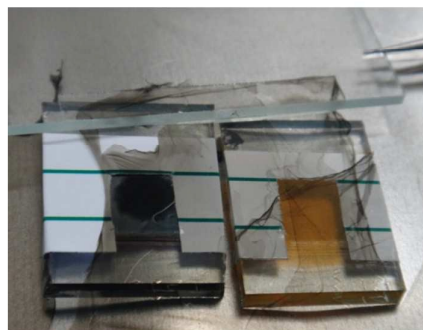
- 1 S. Sun, T. Salim, N. Mathews, M. Duchamp, C. Boothroyd, G. Xing, C.S. Tze, M.L. Yeng, *Energ. Environ. Sci.*, 2014, **7**, 399
- 2 Jr. C.S. Ponseca, T.J. Savenije, M. Abdellah, K. Zheng, A. Yartsev, T. Pascher, T. Harlang, P. Chabera, T. Pullerits, A. Stepanov, J. Wolf, V. Sundstrom, *J. Am. Chem. Soc.*, 2014, **136**, 5189
- 3 S.D. Stranks, G.E. Eperon, G. Grancini, C. Menelaou, M.J.P. Alcocer, T. Leijtens, L.M. Herz, A. Petrozza, H.J. Snaith, *Science*, 2013, **342**, 341
- 4 G. Xing, N. Mathews, S. Sun, S.S. Lim, Y.M. Lam, M. Graetzel, S. Mhaisalkar, T.C. Sum, *Science*, 2013, **342**, 344
- 5 V. D'Innocenzo, G. Grancini, M.J.P. Alcocer, A.R.S. Kandada, S.D. Stranks, M.M. Lee, G. Lanzani, H.J. Snaith, A. Petrozza, *Nat. Commun.*, 2014, **5**,
- 6 W.S. Yang, J.H. Noh, N.J. Jeon, Y.C. Kim, S. Ryu, J. Seo, S.I. Seok, *Science*, 2015, a9272
- 7 N.J. Jeon, J.H. Noh, Y.C. Kim, W.S. Yang, S. Ryu, S.I. Seok, *Nat. Mater.*, 2014,

- 8 J. Im, I. Jang, N. Pellet, M. Gr A Tzel, N. Park, *Nat. Nanotechnol.*, 2014, **9**, 927
- 9 H. Zhou, Q. Chen, G. Li, S. Luo, T. Song, H. Duan, Z. Hong, J. You, Y. Liu, Y. Yang, *Science*, 2014, **345**, 542
- 10 M.M. Lee, J.E.L. Teuscher, T. Miyasaka, T.N. Murakami, H.J. Snaith, *Science*, 2012, **338**, 643
- 11 J. Burschka, N. Pellet, S. Moon, R. Humphry-Baker, P. Gao, M.K. Nazeeruddin, M. Gr A Tzel, *Nature*, 2013, **499**, 316
- 12 L. Mingzhen, M.B. Johnston, H.J. Snaith, *Nature*, 2013, **501**, 395
- 13 Q. Chen, H. Zhou, Z. Hong, S. Luo, H. Duan, H. Wang, Y. Liu, G. Li, Y. Yang, *J. Am. Chem. Soc.*, 2014, **136**, 622
- 14 G.E. Eperon, S.D. Stranks, C. Menelaou, M.B. Johnston, L.M. Herz, H.J. Snaith, *Energ. Environ. Sci.*, 2014, **7**, 982
- 15 H. Choi, J. Jeong, H. Kim, S. Kim, B. Walker, G. Kim, J.Y. Kim, *Nano Energy*, 2014, **7**, 80
- 16 H. Feng, C.C. Stoumpos, H.C. Duyen, R.P.H. Chang, M.G. Kanatzidis, *Nat. Photonics*, 2014, **8**, 489
- 17 J.H. Noh, S.H. Im, J.H. Heo, T.N. Mandal, S.I. Seok, *Nano Lett.*, 2013, **13**, 1764
- 18 Y. Zhao, K. Zhu, *J. Am. Chem. Soc.*, 2014, **136**, 12241
- 19 G.P. Smestad, F.C. Krebs, C.M. Lampert, C.G. Granqvist, K.L. Chopra, X. Mathew, H. Takakura, *Sol. Energ. Mat. Sol. C.*, 2008, **92**, 371
- 20 E. Edri, S. Kirmayer, D. Cahen, G. Hodes, *J. Phys. Chem. Lett.*, 2013, **4**, 897
- 21 E. Edri, S. Kirmayer, M. Kulbak, G. Hodes, D. Cahen, *J. Phys. Chem. Lett.*, 2014, **5**, 429
- 22 R. Seungchan, H.N. Jun, J.J. Nam, C.K. Young, S.Y. Woon, S. Jangwon, I.S. Sang, *Energ. Environ. Sci.*, 2014, **7**, 2614
- 23 A. Mei, X. Li, L. Liu, Z. Ku, T. Liu, Y. Rong, M. Xu, M. Hu, J. Chen, Y. Yang, M. Gratzel, H. Han, *Science*, 2014, **345**, 295
- 24 M. Xu, Y. Rong, Z. Ku, A. Mei, T. Liu, L. Zhang, X. Li, H. Han, *J. Mater. Chem. A*, 2014, **2**, 8607
- 25 Z. Wei, H. Chen, K. Yan, S. Yang, *Angew. Chem. Int. Edit.*, 2014, **53**, 13239
- 26 L. Zhen, J. Yi, W. Jinqun, W. Kunlin, S. Qinke, G. Xuchun, Z. Hongwei, C. Anyuan, W. Dehai, *Journal of Materials Chemistry*, 2010, **20**, 7236
- 27 S.N. Habisreutinger, T. Leijtens, G.E. Eperon, S.D. Stranks, R.J. Nicholas, H.J. Snaith, *Nano Lett.*, 2014, **14**, 5561
- 28 J.H. Heo, D.H. Song, S.H. Im, *Adv. Mater.*, 2014, **26**, 8179
- 29 A. Dymshits, A. Rotem, L. Etgar, *J. Mater. Chem. A*, 2014, **2**, 20776
- 30 A. Dualeh, T. Moehl, N. Tetreault, J. Teuscher, P. Gao, M.K. Nazeeruddin, M. Graetzel, *ACS Nano*, 2014, **8**, 4053
- 31 V. Gonzalez-Pedro, E.J. Juarez-Perez, W. Arsyad, E.M. Barea, F. Fabregat-Santiago, I. Mora-Sero, J. Bisquert, *Nano Lett.*, 2014, **14**, 888
- 32 S. De Wolf, J. Holovsky, S. Moon, P. Lo`pper, B. Niesen, M. Ledinsky, F. Haug, J. Yum, C. Ballif, *The Journal of Physical Chemistry Letters*, 2014, **5**, 1035
- 33 S.A. Kulkarni, T. Baikie, P.P. Boix, N. Yantara, N. Mathews, S. Mhaisalkar, *J. Mater. Chem. A*, 2014, **2**, 9221

Nanoscale

ARTICLE

Electronic Supplementary Information

**Freestanding transparent CNT film****Lifting CNT film****CNT transfer to substrates****Figure S1.** Photos of CNT deposition process.

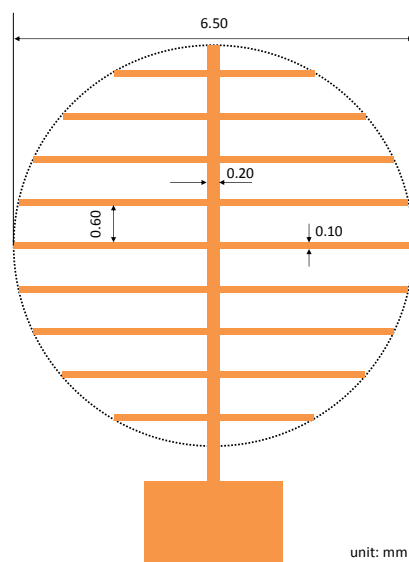


**Figure S2.** Design schematic for evaporated Au finger electrode.

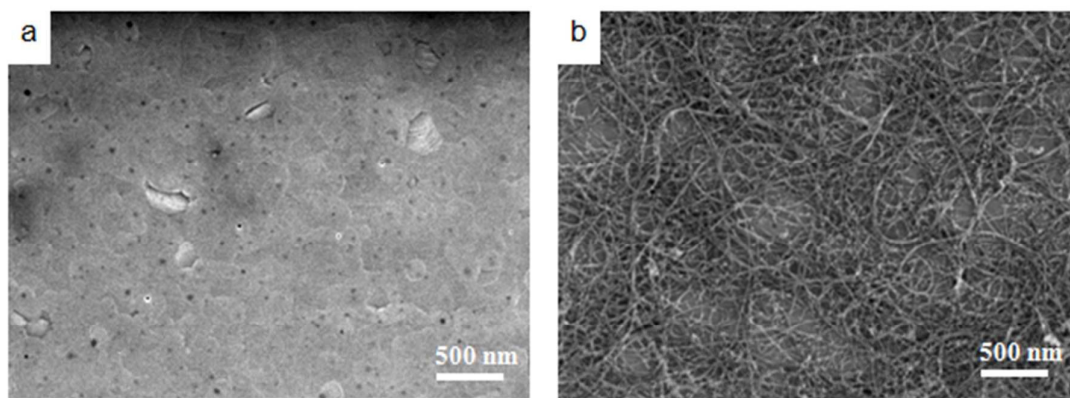


**Figure S3.** (a) Surface SEM image of MAPbBr<sub>3</sub>. (b) SEM image of CNT networks coated on MAPbBr<sub>3</sub> surface.

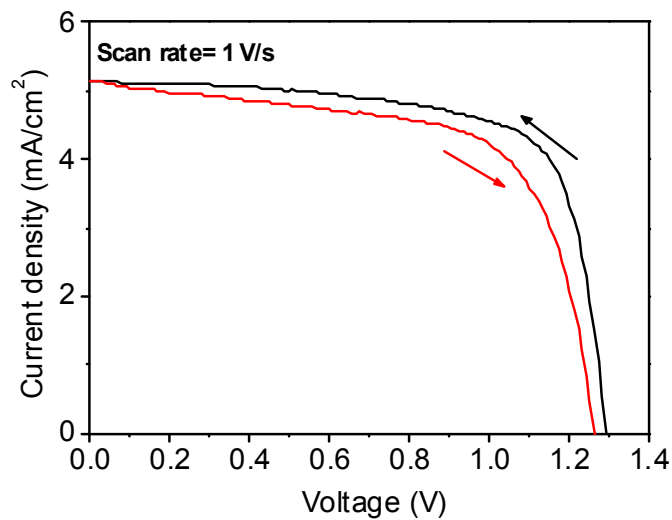


Figure S4. *J-V* hysteresis of MAPbBr<sub>3</sub>/CNT solar cell.

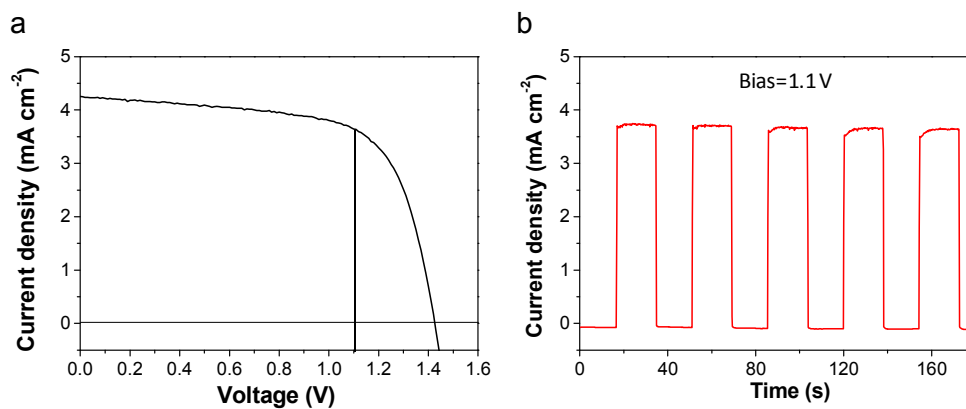


Figure S5. (a) *J-V* curve of a MAPbBr<sub>3</sub>/CNT solar cell; (b) Stable output of the solar cell under 1.0 V bias.

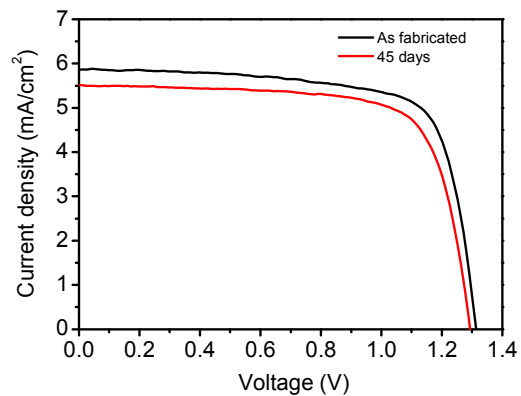


Figure S6. Stability of the MAPbBr<sub>3</sub>/CNTs solar cell stored in desiccator.

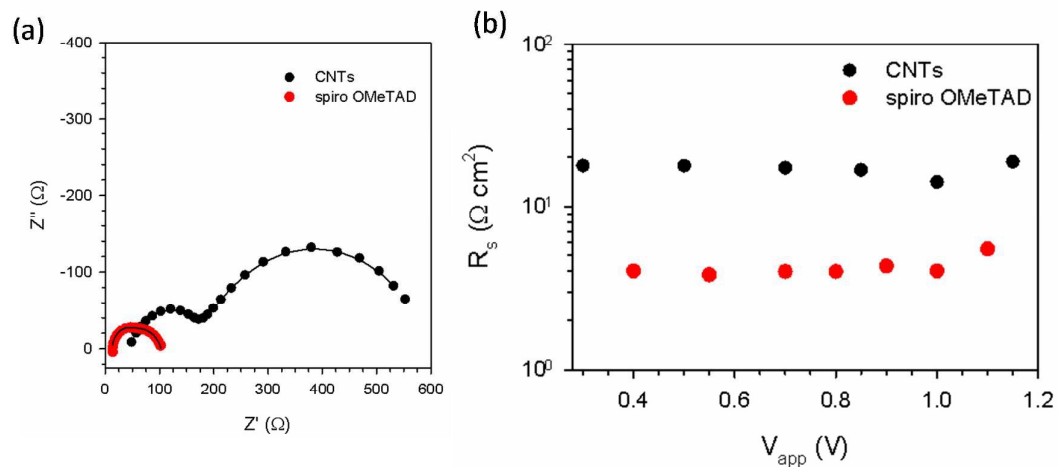


Figure S7 (a) Nyquist plot under illumination and bias of 1.0 V; (b) Series resistance  $R_s$  extracted from the impedance spectra for MAPbBr<sub>3</sub>/CNTs and MAPbBr<sub>3</sub>/spiro-OMeTAD solar cells



**Figure S8.** Photo of semi-transparent MAPbBr<sub>3</sub>/CNT solar cell with gold finger electrode.